20169060

Secondary-side-only Simultaneous Power and Efficiency Control in Dynamic Wireless Power Transfer System

Giorgio Lovison [1)] Daita Kobayashi [1)] Takehiro Imura [2)] Yoichi Hori [1)]

1) The University of Tokyo, Graduate School of Frontier Sciences

5-1-5 Kashiwanoha, Kashiwa, Chiba, 277-8561, Japan

2) The University of Tokyo, Graduate School of Engineering,

7-3-1 Hongo, Bunkyo-ku, Tokyo, 113-8656, Japan

Presented at the EVTeC and APE Japan on May 26, 2016

ABSTRACT: Electric vehicles and wireless power transfer are a convenient combination. Past research considered either power control or efficiency control in wireless secondary side, but a more advanced control is desirable. Therefore, the authors propose a control for power and efficiency with two converters entirely performed on the secondary side of the wireless system, independently from the primary side. In this paper, a dynamic charging scenario is considered: the control must provide the required power at maximum efficiency conditions while the mutual inductance is changing. The experimental results verify that the proposed control effectively works during dynamic charging.

KEY WORDS: dynamic wireless charging, power control, efficiency control

1. INTRODUCTION

In the last few years, electric vehicles (EVs) have become a key point in saving energy, achieving high controllability by use of electric motors and reducing pollution. However, currently most of EVs must be charged via plug-in method: this process is time consuming as well as carrying some safety issues for the consumer such as the high voltage used during charging. Wireless power transfer (WPT) technology recently is becoming suitable for automotive applications. WPT by magnetic resonant coupling[1)] can achieve high power and high efficiency when the transmission distance is lower than one meter because it allows robustness against misalignment, increased air gap and higher transmission efficiency when compared to conventional induction method. There are different types of WPT by magnetic resonant coupling, depending on the compensation carried by the capacitances: one of the types used in automotive application is the series-series (SS) compensation because it allows high power to flow on the receiver side. Currently, static WPT is available on the market; however, developing in-motion wireless power transfer is necessary because it would mean extreme reduction of battery weight and range anxiety; recently, some trial units are been experimented upon and achieved promising results. A good converter control is necessary to send the necessary power to the vehicle with high efficiency[2)]. In WPT, converter control is generally divided into power control and efficiency control; they can be performed on primary side[3) 4)], on secondary side[5) 6)] or on both sides at the same time[7) 8)]. However, most of the times, in past research power and efficiency control have been performed in different sides of the systems (e.g. efficiency control on

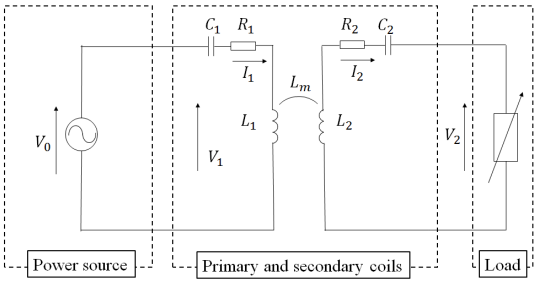

Fig. 1: Equivalent circuit of SS compensated WPT system.

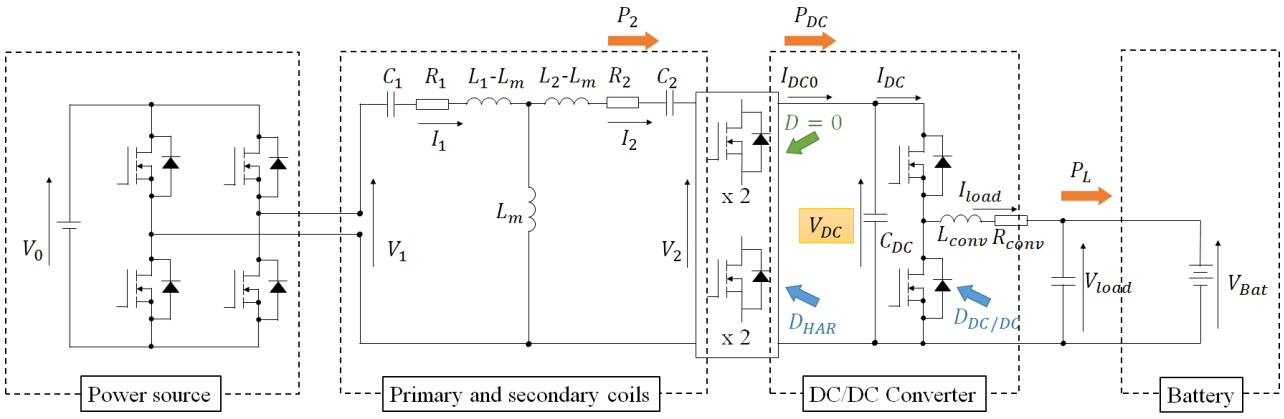

Fig. 2: Reference circuit of WPT using SS compensation and equivalent coil configuration.

primary side and power control on secondary side). A novel control able on the secondary side to transfer at the same time the desired power with high efficiency without any kind of communication with the primary side is desirable. In a WPT system for EV battery charging, the secondary side usually include a rectifier and a DC/DC converter connected to the battery. Therefore, it is possible to control the efficiency and the power flow only by secondary side. The motivation to control only the secondary side consists in keeping the primary side simple, thus allowing a standardization for future commercial WPT installations. A paper dealing with this concept in a static charging scenario has been recently published [9]. Therefore, in this paper, the authors propose a simultaneous power and efficiency control for the secondary side of a WPT system with SS compensation for dynamic charging.

2. CASE OF STUDY

This paper deals with the secondary side control of a WPT system with SS compensation: it includes a half active rectifier (HAR), a DC/DC converter and a battery as load. The frequency in the WPT system is the resonant frequency extracted from the coil parameters and is independent from the load and the distance between the coils. The resonant angular frequency is given as follows:

$$\omega = \sqrt{\frac{1}{L_1 C_1}} = \sqrt{\frac{1}{L_2 C_2}} \tag{1}$$

with L_1 and C_1 as the primary coil inductance and capacitance, respectively; similarly, L_2 and C_2 are the secondary coil inductance and capacitance. The coil internal resistance has no effect on the resonant frequency but affects the losses and the dynamic response of the system. The mutual inductance between the primary and secondary coil depends on factors such as the distance between coils, their geometry, the media between them,

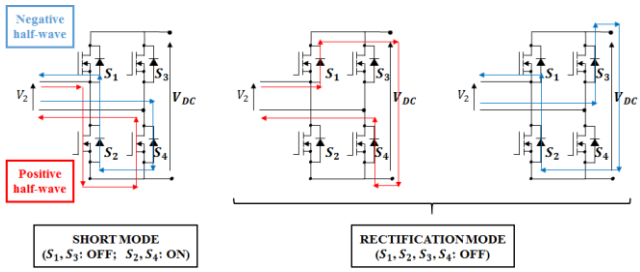

Fig. 3: HAR modes.

the presence of metallic parts in the coils vicinity, etc.. The reference circuit is shown in Fig.1. Using a HAR and a DC/DC converter to control the efficiency and the power flow in the secondary side is proposed with respect to this circuit.

3. PROPOSED CONTROL

3.1. Control concept

In WPT theory, the formulae of the load power P_L and transmitting efficiency η, presented in previous papers [10) 11) 12)], are given respectively by:

$$P_L = \frac{(\omega L_m)^2 Z_L}{\left[R_1(Z_L + R_2) + (\omega L_m)^2\right]^2} V_{1,0}^{\ 2} \tag{2}$$

$$\eta = \frac{(\omega L_m)^2 Z_L}{(R_2 + Z_L)\left[R_1(Z_L + R_2) + (\omega L_m)^2\right]} \tag{3}$$

where Z_L is the load impedance seen from the secondary coil, R_2 is the secondary coil resistance, R_1 is the primary coil resistance, L_m is the mutual inductance between the coils and $V_{1,0}$ is the rms value of the fundamental wave of primary side voltage. In this paper, the power factor of the primary side voltage is assumed to be unity, therefore the power factor of the fundamental wave of the secondary side voltage V_2 is considered to be unity, too. The HAR is a full wave diode bridge whose low side diodes are replaced by active devices like

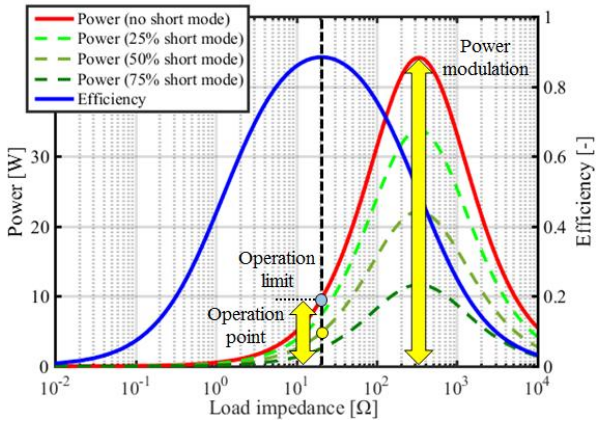

Fig. 4: Transmission efficiency and load power with respect to load impedance for $V_1 = 20\,\mathrm{V}$ and $L_m = 39.2\,\mu\mathrm{H}$.

MOSFETs or IGBTs: by turning on the both the devices on the low side, the coil terminals are shorted (short mode) and no power is transmitted to the load. Since the SS compensation of magnetic resonant coupling makes the secondary side coil behave like an equivalent current source, short-circuiting the coil terminals is allowed. On the other hand, if both the low side devices are off, the converter works like a single-phase rectifier composed by diodes (rectification mode), as shown in Fig. 3, and power is sent to the load.

The influence of load impedance has been examined in [10) 11) 13)]. In particular, the load impedance associated with maximum transmission efficiency and the one related to maximum deliverable power are different. The former one is equal to:

$$Z_{L,\eta\max} = \sqrt{\frac{R_2}{R_1}(\omega L_m)^2 + {R_2}^2} \tag{4}$$

The secondary coil voltage that maximizes the transmission efficiency can be expressed by:

$$V_{\eta\max} = \sqrt{\frac{R_2}{R_1}}\,\frac{\omega L_m}{\sqrt{R_1 R_2} + \sqrt{R_1 R_2 + (\omega L_m)^2}}\,V_{1,0} \tag{5}$$

On the other hand, the load impedance and the secondary coil voltage related to the maximum available power are given by:

$$Z_{L,P\max} = \frac{(\omega L_m)^2}{R_1} + R_2 \tag{6}$$

$$V_{P\max} = \frac{\omega L_m}{2R_1} V_{1,0} \tag{7}$$

Voltages in (5) and (7) are rms values of the fundamental wave component. Finally, the total input impedance seen from the secondary coil must be $Z_{L,\eta\max}$ during rectification mode. On the other hand, when short mode happens the secondary input impedance is only a few ohms. The control of the input

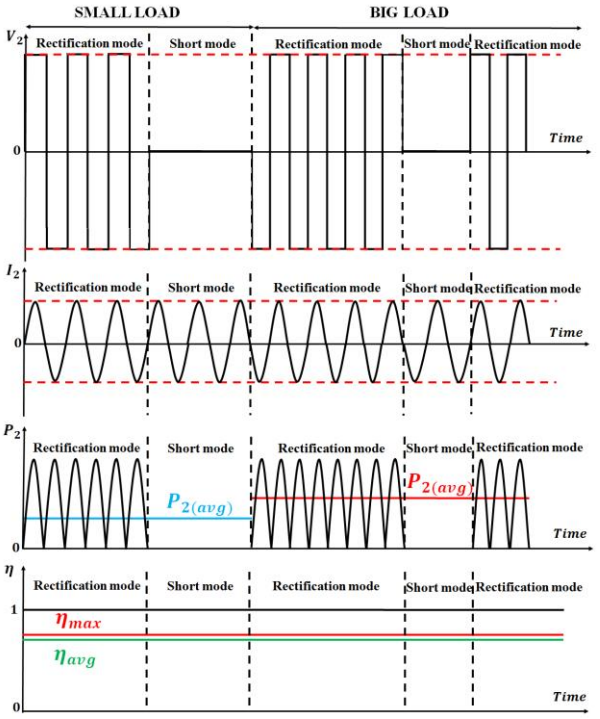

Fig. 5: Control concept with parameters waveforms (top to bottom: HAR input voltage V_2, HAR input current I_2, HAR input power P_2, total efficiency η).

impedance allows to use the HAR to send the power desired by the load to the DC/DC converter, which in turn is used to guarantee maximum transmitting efficiency. Fig. 4 shows the relationship between power and efficiency with respect to the load impedance. The power corresponding to maximum transmitting efficiency is fixed. However, by the proposed secondary side control, it is possible to send a different power value while retaining the same transmitting efficiency. This is because of the switching between short mode and rectification mode by HAR. The length of the short mode during the HAR switching period determines the amount of power received by the load. Fig. 5 shows how the control works and how the secondary side input parameters are shaped. In rectification mode, the rms value of secondary side voltage is unchanged, therefore the rms value of the secondary side input power is unchanged. The secondary side coil behaves like an equivalent current source so the current does not change as well. The power is calculated by averaging, as well as the efficiency; consequently, the averaged efficiency computed from the ratio between secondary power and primary power will be lower because of the resistive losses happening during short mode. In fact, during rectification mode the efficiency is maximum while in short mode it is zero since the load is not supplied.

3.2. Control operation

In Fig. 6 and Fig. 7 are represented the control blocks for the HAR and DC/DC converter, respectively. The feedback part of both the controllers is designed with the pole placement method.

$$C_{PID}(s) = k_p + \frac{k_i}{s} + \frac{k_d s}{\tau s + 1} \tag{8}$$

The HAR can be thought as a non-linear resistance; however, in this paper dynamic charging is considered, therefore transient must be included. Then, its plant includes only one pole due to secondary DC smoothing capacitor C_{DC}:

$$P_{HAR}(s) = \frac{P_{DC}(s)}{d(s)} = \frac{P_2}{1 + R_L C_{DC} s} \tag{9}$$

with P_2 as the HAR input power and R_L as the equivalent circuit load resistance. However, instead of a PID controller, a PI one is considered sufficient. In the proposed control, the following requirements must be met:

1) Primary side voltage source and system frequency are given and fixed. The duty cycle of the primary converter is fixed, consequently the primary coil voltage is fixed, too.

2) The HAR switching frequency is at least one order of magnitude lower than the DC/DC converter one to avoid operation conflict and potential instability.

3.2.1 HAR control

The HAR modulates the power by adjusting the duty cycle to switch between rectification mode and short mode. Therefore, a voltage formula related to the desired power P_L^* and the maximum power is necessary. From (7), the above mentioned voltage is computed as follows [14]:

$$V_{P_L^*} = V_{P\max} - \sqrt{V_{P\max}{}^2 - \frac{\left[R_1 R_2 + (\omega L_m)^2\right] P_L^*}{R_1}} \tag{10}$$

By rearranging (10), the value of the desired power as a function of the voltage is obtained as follows:

$$P_L^* = \frac{R_1\left[V_{P\max}{}^2 - \left(V_{P_L^*} - V_{P\max}\right)^2\right]}{R_1 R_2 + (\omega L_m)^2} \tag{11}$$

Since the aim is to achieve high transmission efficiency, the upper limit of the desired power is reached when $V_{P_L^*}$ is equal to $V_{\eta\max}$; therefore, (11) is adjusted and becomes:

$$P_{L,\eta\max} = \frac{R_1\left[V_{P\max}{}^2 - \left(V_{\eta\max} - V_{P\max}\right)^2\right]}{R_1 R_2 + (\omega L_m)^2} \tag{12}$$

The feedforward part of the control in Fig. 6 is decided by the ratio between the HAR input power P_2 and (12).

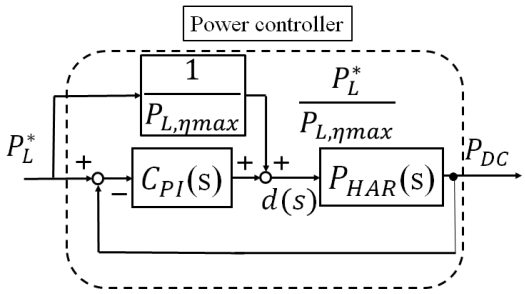

Fig. 6: HAR power control block.

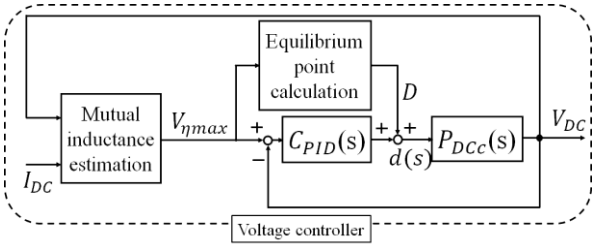

Fig. 7: DC/DC converter DC link efficiency control block.

3.2.2 DC/DC converter control

In this paper, a buck converter is considered. The control makes the DC link voltage equal to the maximum efficiency voltage, but the mutual inductance must be known. Since this paper deals with a dynamic charging scenario, the coils are moving and therefore the mutual inductance changes. Therefore, a method to estimate the mutual inductance is necessary. In [15], a real-time estimation of the coupling coefficient by using secondary side DC link information and recursive least square (RLS) filter has been proposed. In this paper, the DC/DC converter control concept is the same. The estimation is important to the control because it affects also the HAR control: in fact, in (12) there are many factors related to it. Poor estimation leads to noisy, unstable references that severely reduce the efficiency. In particular, the operation of HAR is the main cause of noisy estimation. This is because during short mode the DC link current is equal to zero: since the secondary DC current information is used as input in the RLS filter, when its value becomes zero so does the estimated mutual inductance and the voltage reference for high efficiency control. The RLS filter output $y[i]$ and input $\varphi[i]$ are expressed as follows [15]:

$$y[i] = V_1 + \sqrt{V_1^2 - 4R_1 I_{DC}(V_{DC}[i] + R_2 I_{DC}[i])} \tag{13}$$

$$\varphi[i] = 2I_{DC}[i]\omega \tag{14}$$

with i as the sampling counter. From (13) and (14), the updating parameters are computed in discrete time as:

$$\varsigma[i] = y[i] - (\varphi[i]\theta[i-1]) \tag{15}$$

Table 1: Circuit parameters.

Parameter	Value
Load battery voltage [V]	6.34
Primary coil capacitance C_1 [nF]	6.03
Secondary coil capacitance C_2 [nF]	12.15
DC link capacitor C_{DC} [μF]	1000
Primary coil inductance L_1 [μH]	417.8
Secondary coil inductance L_2 [μH]	208.5
Mutual inductance L_m [μH] (best alignment)	39.2
Coil gap [mm] (best alignment)	100
Resonant frequency [kHz]	100
Primary coil resistance R_1 [Ω]	1.83
Secondary coil resistance R_2 [Ω]	1.281

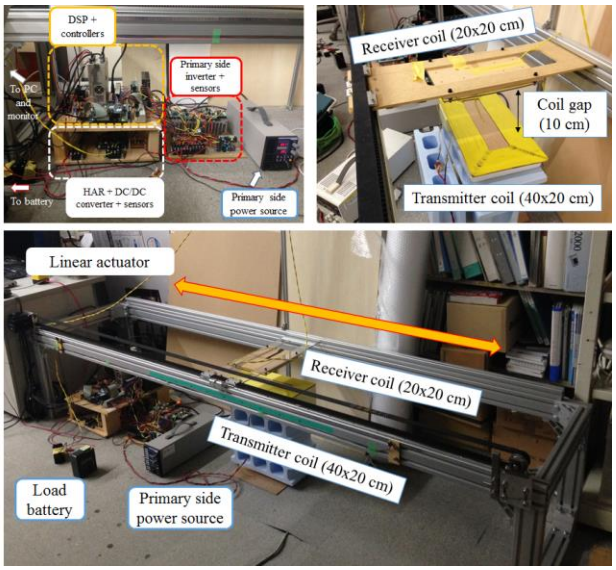

Fig. 8: Experimental setup.

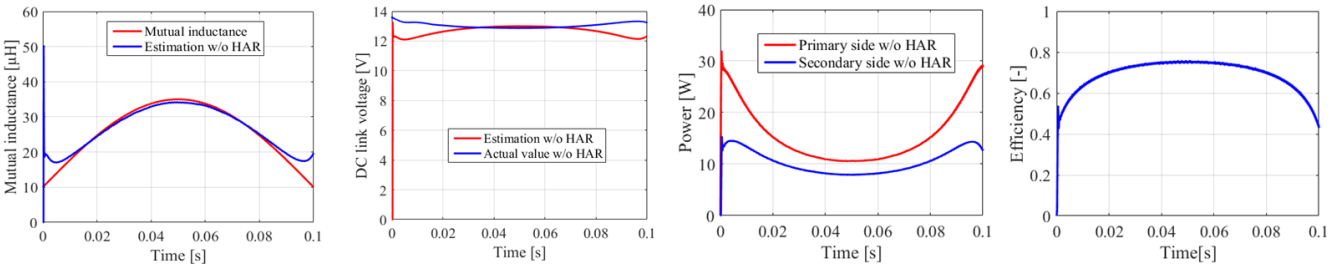

(a) Mutual inductance (b) DC link voltage (c) Power (d) DC to DC efficiency

Fig. 9: Simulation result with the DC/DC converter control proposed in [15] for a speed of 10 km/h.

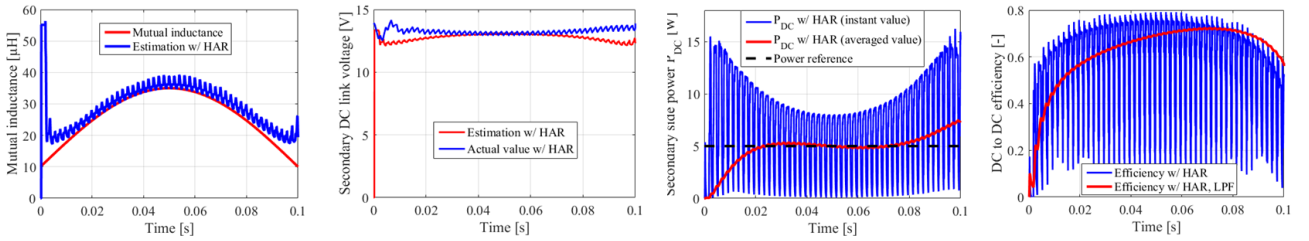

(a) Mutual inductance (b) DC link voltage (c) Secondary side power (d) DC to DC efficiency

Fig. 10: Simulation result with the proposed control: reference power is 5 W and the speed is 10 km/h.

$$\theta[i] = \theta[i-1] + \frac{T[i-1]\varphi[i]}{\lambda + \varphi[i]^2 T[i-1]}\varsigma[i] \tag{16}$$

$$T[i] = \frac{T[i-1]}{\lambda}\left(1 - \varphi[i]\frac{T[i-1]\varphi[i]}{\lambda + \varphi[i]^2 T[i-1]}\right) \tag{17}$$

However, in this paper ,the application of conditional updating to the RLS filter is considered: when short mode happens, the values are held at their last value; when rectification mode happens, the filter coefficients updating restarts. These parameters are employed in the PID feedback and in the feedforward equilibrium point as described in [15]. Finally, the transient of the current I_2 must end much earlier than the vehicle speed one because the filter can be applied only in steady state.

4. SIMULATION AND EXPERIMENTAL RESULT

In order to verify the effectiveness of the proposed method, experiments have been performed. The aim is to prove that even if mutual inductance changes, the control is stable and the desired power is effectively sent to the load. The circuit parameters are reported in table 1. The DC/DC converter resistance R_{conv} and its inductance L_{conv} are 0.2 Ω and 1000 μH, respectively; as for the DC/DC converter filter capacitance C_{conv}, its value is 1000 μF. The HAR switching frequency is 500 Hz, while the DC/DC converter one is 10 kHz. In order to verify the proposed system, a mini model is being used. The primary voltage source is 18 V. The experimental setup is shown in Fig. 8. In the experiment, the

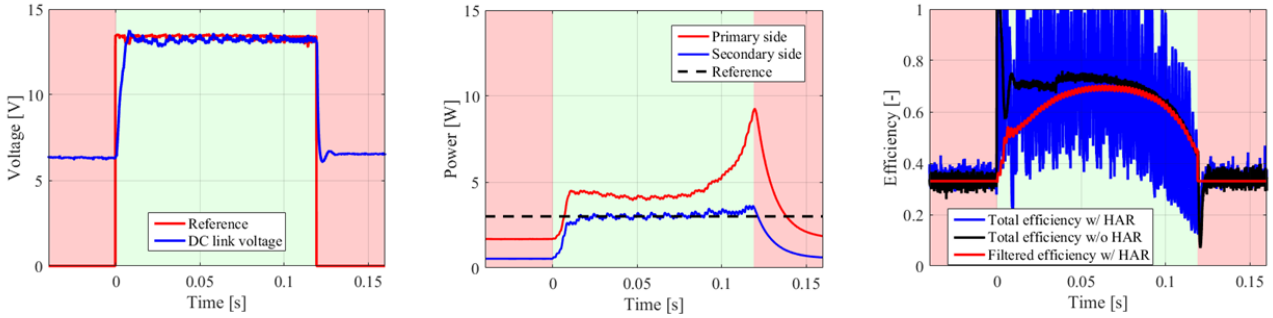

(a) DC link voltage (b) Power (c) DC to DC efficiency

Fig. 11: Experiment result with the proposed control: reference power is 3 W and the speed is 10 km/h.

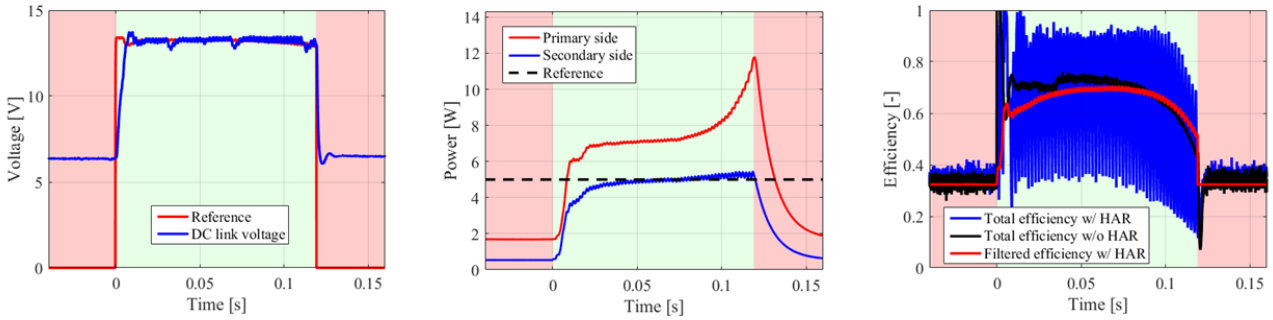

(a) DC link voltage (b) Power (c) DC to DC efficiency

Fig. 12: Experiment result with the proposed control: reference power is 5 W and the speed is 10 km/h.

receiver coil is moved by a linear actuator. The position of the coil is recorded by an encoder, which transmits the data to the controller. The speed by which the receiver coil moves is 10 km/h. The experimental results on DC to DC efficiency are compared with the experimental results obtained by using the control and the converters presented in [15]. The experiments for a desired power of 3 W and 5 W have been performed.

In Fig. 9, the simulation results using the method and the converters proposed in [15] are shown. In these simulation, the full bridge diode rectifier is considered instead of the HAR in order to to provide a reference for the transmitted power and efficiency. In fact, if using a diode rectifier, the power is not controlled. The efficiency in Fig. 9(d) is assumed to be the maximum DC to DC efficiency the system can reach in ideal conditions.

In Fig. 10, the simulation result of the proposed control are presented. The influence of short mode is very noticeable. The desired power is sent to the load and high efficiency is achieved. However, in 12(c), the filtered average value is higher than the actual value. This is due to the filter delay and the HAR low switching frequency. Unfortunately, the mutual inductance estimation results in the experiment are not as good as the ones described in [15]. Nevertheless, with those results the control can still achieve the expected desired power and high efficiency, as it can be seen in Fig. 11 and Fig. 12.

In Fig. 11, the experimental results for a required power of 3 W are shown. In 11(a), the DC link voltage reference and its actual value are shown. The voltage reference is computed from the mutual inductance value and the actual voltage can match its reference. As it can be seen from 11(b), the DC link power is around 3 W, the reference value. The values of the power are filtered with weighted moving average, therefore the graphic shows the averaged value. When the coupling coefficient becomes lower due to the coil movement, there is a power surge typical of dynamic charging. The transmitted power matches the reference when the mutual inductance is at its maximum value. In Fig. 11(c), the DC to DC efficiency is shown. The blue line represents its true value, while the red line is the filtered value. In fact, during short mode, the efficiency falls drastically to extremely low values; actually, in the experimental setup there is an offset on the sensors, therefore the efficiency is not shown to become zero. On the other hand, when rectification mode happens, the current transient causes the values of the actual efficiency to be higher than the theoretical values: this is only a computational error and has no relevance. The averaged efficiency value is very close to the maximum efficiency value, represented by the black line. The difference in efficiency is due to the losses generated during short mode. These losses are small because of the low power experiment.

The experimental results with a desired power of 5 W are presented in Fig. 12. In 12(b) and 12(c), the graphic shows filtered averaged values, too.

As expected, in both the experiment efficiency measurements the filtered value of the efficiency is higher than the actual value, just like in 10(d). The reason is the same as explained before. The results in both cases show that desired power and high efficiency are achieved, thereby proving the effectiveness of the control.

5. CONCLUSION

The authors proposed a simultaneous power control and efficiency control to be performed only on the secondary side of a wireless power transfer system, independently from the primary side, by using a HAR and a DC/DC converter. In this paper, a dynamic wireless power transfer scenario is considered. By adopting an already proposed mutual inductance estimation concept, experiments have been carried out. Experimental results verified the effectiveness of the proposed method since the power reference is matched and high efficiency is achieved.

Future works include high power experiment and mutual inductance estimation improvement.

REFERENCES

(1) A. Kurs, A. Karalis, R. Moffatt, J.D. Jonnopoulos, P. Fisher, M. Soljacic : Wireless power transfer via strongly coupled magnetic resonances, Science Expressions on 7 June 2007, Vol. 317, No. 5834, pp. 83-86 (2007).

(2) S. Li, C.C. Mi: Wireless power transfer for electric vehicle applications, IEEE Journal of Emerging and Selected Topics in Power Electronics, pp. 1-14 (2013).

(3) H. L. Li, A. P. Hu, G. A. Covic, T. Chunsen: A new primary power regulation method for contactless power transfer, IEEE International Conference on Industrial Technology (ICIT), pp. 1-5 (2009).

(4) J. M. Miller, C. P. White, O. C. Onar, P. M. Ryan: Grid side regulation of wireless power charging of plug-in electric vehicles, IEEE Energy Conversion Congress and Exposition (ECCE), pp. 261-268 (2012).

(5) W. Chwei-Sen, O. H. Stielau, G. A. Covic: Design considerations for a contactless electric vehicle battery charger, IEEE Transactions on Industrial Electronics, vol. 52, pp. 1308-1314 (2005).

(6) M. Fu, C. Ma, X. Zhu: A cascaded boost-buck converter for high efficiency wireless power transfer systems, IEEE Transactions on Industrial Informatics, Vol. 10, No. 3, pp. 1972-1980 (2014).

(7) H.H. Wu, A. Gilchrist, K. D. Sealy, D. Bronson: A high efficiency 5 kW inductive charger for EVs using dual side control, IEEE Transactions on Industrial Informatics, vol. 8, pp. 585-595 (2012).

(8) T. Diekhans, R. W. De Doncker: A dual-side controlled inductive power transfer system optimized for large coupling factor variations, IEEE Energy Conversion Conference and Exposition (ECCE) 2014, pp. 652-659 (2014).

(9) G. Lovison, M. Sato, T. Imura, Y. Hori: Secondary-side-only Control for Maximum Efficiency and Desired Power in Wireless Power Transfer System, Proceedings of 41st Annual Conference of the IEEE Industrial Electronics Society (IECON) 2015, pp. 4965-4970 (2015).

(10) K. Hata, T. Imura and Y. Hori: Maximum Efficiency Control of Wireless Power Transfer Considering Dynamics of DC-DC Converter for Moving Electric Vehicles, The Applied Power Electronics Conference and Exposition, pp. 3301-3306, (2015).

(11) T. Hiramatsu, X. Huang, M. Kato, T. Imura and Y. Hori: Wireless Charging Power Control for HESS Through Receiver Side Voltage Control, The Applied Power Electronics Conference and Exposition (APEC), pp. 1614-1619 (2015).

(12) M. Kato, T. Imura, Y. Hori: New characteristics analysis considering transmission distance and load variation in wireless power transfer via magnetic resosnat coupling, IEEE Proceedings INTELEC (2012).

(13) M. Kato, T. Imura, Y. Hori: Study on maximizing efficiency by secondary side using DC-DC converter in wireless power transfer via magnetic resosnat coupling, EVS27, pp. 1-5 (2013).

(14) K. Hata, T. Imura, Y. Hori: Dynamic Wireless Power Transfer System for Electric Vehicle to Simplify Ground Facilities - Power Control Based on Vehicle-side Information, The 28th International Electric Vehicle Symposium and Exhibition (EVS), pp. 1 – 12 (2015)

(15) D. Kobayashi, T. Imura, Y. Hori: Real-time coupling coefficient estimation and maximum efficiency control on dynamic wireless power transfer for electric vehicles, 2015 IEEE PELS Workshop on Emerging Technologies: Wireless Power, pp. 1-6 (2015).